Journal of Electrical and Computer Engineering Innovations
(JECEI)
Journal homepage: http://www.jecei.sru.ac.ir

Research paper

Robust Linear Parameter Varying Fault Reconstruction of Wind Turbine Pitch Actuator Using Second-Order Sliding Mode Observer

M. Mousavi[1], M. Ayati[2,], M. Hairi-Yazdi[2], S. Siahpour[3]*

[1]*Department of Mechanical Engineering, Binghamton University, Binghamton 13902, USA.*

[2]*School of Mechanical Engineering, College of Engineering, University of Tehran, Tehran, Iran.*

[3]*Department of Mechanical Engineering, University of Cincinnati, Cincinnati 45221, USA.*

Article Info

Article History:
Received 15 June 2022
Reviewed 29 July 2022
Revised 19 August 2022
Accepted 26 September 2022

Keywords:
Wind turbines
Pitch actuator faults
Linear parameter varying model
Sliding mode observer
Fault reconstruction

[*]Corresponding Author's Email Address: *m.ayati@ut.ac.ir*

Abstract

Background and Objectives: In this paper, a novel linear parameter varying (LPV) model of a wind turbine is developed based on a benchmark model presented by Aalborg University and KK-electronic a/c. The observability and validity of the model are investigated using real aerodynamic data.
Methods: In addition, a robust fault detection and reconstruction method for linear parameter varying systems using second-order sliding mode observer is developed and implemented on the linear parameter varying model. The fault signal is reconstructed using a nonlinear term named equivalent output error injection during sliding motion and a proper transformation. The effect of uncertainties and incorrect measurements are minimized by employing an oriented method that requires solving a nonlinear matrix inequality. During numerical simulations, an actuator fault in the pitch system is considered and the performance of the method in fault reconstruction is investigated.
Results: Wind speed range is considered from 14 m/s to 16 m/s and it is regarded as a stochastic input exerting aerodynamic torque. Fast and accurate fault reconstruction happens in 0.6 seconds with less than one percent error. The observer performance is not affected by the fault and fault is estimated in 2.5 seconds with an error smaller than 2.48 percent.
Conclusion: Results illustrate fast and accurate fault reconstruction and accurate state estimations in the presence of actuator fault.
In this paper, a novel linear parameter varying (LPV) model of a wind turbine is developed based on a benchmark model presented by Aalborg University and KK-electronic a/c. The observability and validity of the model are investigated using real aerodynamic data. In addition, a robust fault detection and reconstruction method for linear parameter varying systems using a second-order sliding mode observer is developed and implemented on the linear parameter-varying model. The fault signal is reconstructed using a nonlinear term named equivalent output error injection during sliding motion and a proper transformation. The effect of uncertainties and incorrect measurements are minimized by employing an H_∞ oriented method which requires solving a nonlinear matrix inequality. During numerical simulations, an actuator fault in the pitch system is considered, and the performance of the method in fault reconstruction is investigated. Wind speed range is considered from 14 m/s to 16 m/s and it is regarded as a stochastic input exerting aerodynamic torque. Fast and accurate fault reconstruction happens in 0.6 seconds with less than one percent error. The observer performance is not affected by the fault and fault is estimated in 2.5 seconds with an error smaller than 2.48 percent results illustrate fast and accurate fault reconstruction and accurate state estimations in the presence of actuator fault.

Introduction

The costs of wind turbines consist of two parts of implementation and maintenance. The maintenance of large wind turbines is a time-consuming process [1], and a costly procedure, especially in offshore wind farms. It requires the generator disconnection from the power distribution network. Therefore, designing and utilizing a fault detection and isolation (FDI) system to diagnose, isolate, and reconstruct wind turbine faults is highly beneficial and critical in supervisory and maintenance cost reduction. In addition, it increases the lifetime of the turbine components and enhances the power generation due to the fault accommodation and active fault-tolerant control in which a reconfigurable controller is employed to accommodate the effect of faults [2]-[6].

The faults occurring in a large wind turbine are classified into three categories. Sensor faults which include rotor speed, generator speed, generator torque, and pitch angle and they, appear as biased output, random output, fixed output, or no output as discussed in [7]. Component faults such as drive train deficiency [8], mass imbalance of the rotor [9], and the generator system [10] are included in the second class. The third category of wind turbine faults aims at the actuator faults, such as the pitch actuator fault, which is addressed in this paper. The pitch system is responsible for the adjustment of the pitch angle of the rotor blades for the variable-pitch wind turbines. Such systems are important in terms of the amount of wind power captured by blades.

Two types of pitch control systems are used in variable-pitch wind turbines. In the first type, three individual electrical motors are implemented. This is beneficial for the fast reaction of the turbine to wind speed changes and power demand. The second type consists of three individual hydraulic pumps, which are slower but bear more stiffness and have smaller backlash. Therefore, considering large wind turbines, a hydraulic pitch system is suggested for higher reliability. Pitch actuator faults occur for three reasons such as high air content of oil, pump wear, and hydraulic leakage. Hydraulic leakage is an incipient fault and occurs faster compared to the other faults. Thus, it should be considered to reduce cost and energy consumption, decrease operational load, increase power harvesting, and avoid stalling [8], [11]-[13], [37], [38].

The rate of occurrence and the values of faulty and healthy properties are shown in the corresponding columns of Table 1. The state of $\theta = 0$ represents proper situation and $\theta = 1$ is fully faulty operation [7]. In the case of hydraulic fault incidence in each of the individual pitch systems, control efforts may lead to two decisions: (1) generator power exceeds the nominal value (2) output power is reduced, which results in power efficiency reduction. As a result of the leakage in the pitch system, the actuation of the pitch angle becomes slower, and smaller wind power is captured. As a result, fault detection, reconstruction, and fault accommodation are useful decisions to reinforce the control system in a way that energy-related cost functions are satisfied [2]-[6]. Many research projects such as the current work have been conducted for this issue to improve the estimation speed and accuracy of the observer-based fault diagnosis methods [2], [3], [6].

Table 1 Rate of incidence and values of faulty and healthy properties in pitch hydraulic system

	Faulty operation	Rate of fault incidence
No-fault	$\omega_n = 11.11\ rad/s, \zeta = 0.6$	
High air content	$\omega_n = 5.73\ rad/s, \zeta = 0.45$	$\lvert\dot{\theta}\rvert \approx 1/month$
Pump wear	$\omega_n = 7.27\ rad/s, \zeta = 0.75$	$\lvert\dot{\theta}\rvert \approx 1/(20\ years)$
Hydraulic leakage	$\omega_n = 3.42\ rad/s, \zeta = 0.9$	$\lvert\dot{\theta}\rvert \approx 1/(100\ seconds)$

The wind turbine benchmark considered in this paper is developed by Aalborg University and KK-electronic a/c, enabling the simulation of various sensor and actuator faults [14]. This model is nonlinear due to the relation of wind and aerodynamic torque exerting on wind turbine blades. This kind of nonlinearity has been handled in different methods. Linearizing around one or several operating points and switching among them (gain-scheduling control) [15] is one of these methods. In this method, several observers are designed in which for reducing switching effects, bumpless switching between models should be considered. Linear parameter varying (LPV) modelling is another method where nonlinear terms are turned into linear but time-varying parameters (quasi-linear) [16]-[18]. In such methods, nonlinear terms are expressed in LPV form. Generally, LPV models yield higher accuracy for the all operating points. Using LPV models leads to LPV observer design; thus, the advantages of linear system characteristics could be utilized.

In this paper, fault detection and reconstruction are covered. An LPV model of the wind turbine is developed and a model-based robust second-order sliding mode observer is applied to the LPV wind turbine model. LPV model is valid in the entire operating trajectory and does not require linearization around one or several operating point(s) [19]-[24]. Once the observer gains are obtained, the observer and fault reconstruction formula are

attainable for all the wind turbine operating regions. Actually, LPV methods attempt to parametrize the model closer to real world at the cost of larger computational effort and complication. Model-based methods are preferable in fault detection and reconstruction studies where physical components' parameters of the plant are accessible. Some surveys in model-based wind turbine FDI have been carried out in [22], [24]-[32].

The proposed observer of this paper includes an LTI gain for linear output error signal and an LPV gain for nonlinear residual signals. The reconstructed actuator fault is generated once the sliding motion takes place using a nonlinear residual signal called "equivalent output injection". Observer design matrices are obtained using H_∞ concepts and solving a nonlinear matrix inequality in which the effect of uncertain and imperfect measurements is minimized.

This paper is structured as follows. Section 2 describes the wind turbine benchmark model. Section 3 presents the development of the methodology and observer design procedure. Then, the pitch actuator fault description is presented in Section 4. Section 5 explains the LPV system description and Section 6 is dedicated to numerical results and energy analysis. Finally, Section 7 is the conclusion.

Wind turbine benchmark model

An overview of the wind turbine model in the benchmark developed by Aalborg University and KK-electronic a/c [14] is illustrated in Fig. 1. The variables are introduced in the following subsections.

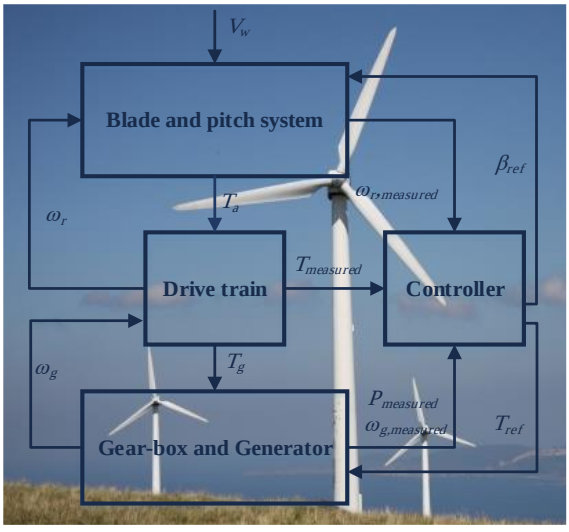

Fig. 1: Wind turbine benchmark developed by Aalborg University and KK-electronic a/c (background photo [31]).

Using aerodynamic principles, the correlation between the wind speed, rotor speed, blades' pitch angle, and the aerodynamic torque exerting the blades is shown in (1). The mentioned correlation is derived considering two assumptions.

1. The wind speed is constant all over the surface of the blades.

2. The wind speed is perpendicular to the rotor plane.

ρ_{air}, R, $\beta(t)$, $\omega_r(t)$, and $V_w(t)$ are air density, blade radius, pitch angle, rotor speed, and average wind speed, respectively. $\lambda(t)$ is the tip speed ratio which is defined in (2). The aerodynamic torque is approximated in (1) using a factor named aerodynamic torque coefficient $C_q(\lambda(t),\beta(t))$.

$$T_a = \frac{\rho_{air}\,\pi R^3 C_q(\lambda,\beta) V_w^2}{2} \tag{1}$$

$$\lambda(t) = \frac{R\omega_r(t)}{V_w(t)} \tag{2}$$

The pitch system consists of three identical hydraulic pumps as the actuator for adjusting the blades' angle by rotation. Three internal controllers are adopted for each actuator giving proper input signals to the actuators. In addition, a second-order transfer function is considered for each of the pitch actuators correlating control input (β_{ref}) to the pitch angle (β). The damping ratio and natural frequency of this model are $\zeta(t)$ and $\omega_n(t)$, respectively. These properties might be time-varying in the event of faults for each system. β_{ref} is pitch control input signal entering each pitch actuator.

$$\begin{aligned}\ddot{\beta}(t) = &-2\zeta(t)\omega_n(t)\dot{\beta}(t) + \omega_n^2(t)\beta_{ref} \\ &- \omega_n^2(t)\beta(t)\end{aligned} \tag{3}$$

The drive-train of the wind turbine consists of two shafts as the low-speed (driver) and the high-speed shaft (driven). The shafts are connected using a gear-box and the aerodynamic power is transferred to the generator through a high-speed shaft. The coupled dynamic equations of the shafts which are considered as a mass-spring model are expressed in (4), (5).

$$\begin{aligned}J_r\,\dot{\omega}_r(t) = &\,T_a(\omega_r,\beta,V_w,t) - K_{dt}\,\theta(t) \\ &- (B_{dt} + B_r)\omega_r(t) \\ &+ \frac{B_{dt}}{N_g}\omega_g(t)\end{aligned} \tag{4}$$

$$\begin{aligned}J_g\dot{\omega}_g\,(t) = &\frac{\eta_{dt}K_{dt}}{N_g}\theta(t) + \frac{\eta_{dt}B_{dt}}{N_g}\omega_r(t) \\ &- \left(\frac{\eta_{dt}B_{dt}}{N_g^2} + B_g\right)\omega_g(t) \\ &- T_g\end{aligned} \tag{5}$$

$$\dot{\theta}(t) = \omega_r(t) - \frac{1}{N_g}\omega_g(t) \tag{6}$$

where, ω_r, ω_g are the rotor and generator speeds, respectively, $\theta(t)$ is the torsion angle of the drive train, T_g is generator torque, J_r and J_g are rotor and generator moments of inertia, K_{dt} and B_{dt} are torsional stiffness

and damping, B_r and B_g are the rotor and generator viscous friction, N_g is the gear ratio and η_{dt} is the efficiency of drive-train. The generator and converter subsystem are modeled by first-order transfer functions:

$$\frac{T_g(s)}{T_{g,ref}(s)} = \frac{\alpha_{gc}}{s + \alpha_{gc}} \tag{7}$$

where, α_{gc} is the generator and converter model parameter and $T_{g,ref}$ is the control output signal of the converter. Parameter values of the benchmark are: $J_r = 55e6$ kg. m^2, $K_{dt} = 2.7e9$ m/rad, $B_g = 3.034$ N. m. s/rad, $N_g = 95$, $\eta_{dt} = 0.92$, $R = 57.5$ m, $J_g = 390$ kg. m^2, $\rho_{air} = 1.225$ kg/m^3, $B_r = 27.8$ kNm/(rad/s), $B_{dt} = 945$ kN. m/(rad/s).

Observer Design

Nowadays, condition monitoring is attracting more attention in technology advancements. It is implemented to prevent serious failures by detecting faults. Condition monitoring in advanced engineering instruments analyses the deviations from normal conditions and detects the existence of faults and failures. On the other hand, Fault reconstruction is an online fault detection method that offers additional information about the size, location, and severity of faults. Such data are useful in the choice of proper action during faulty conditions. Moreover, control efforts are configured considering reconstructed fault data (fault accommodation) to provide better performances during faulty conditions.

A. LPV System Description

An uncertain LPV plant that is subjected to actuator faults is described by

$$\begin{aligned} \dot{x}(t) &= A(\boldsymbol{\rho})x(t) + B(\boldsymbol{\rho})u(t) + M(\boldsymbol{\rho})f_i(t) \\ &\quad + Q\xi(\boldsymbol{\rho}, x, t) \\ y(t) &= Cx(t) + \vartheta(t) \end{aligned} \tag{8}$$

where, $A(\boldsymbol{\rho}) \in \boldsymbol{R}^{n\times n}$, $B(\boldsymbol{\rho}) \in \boldsymbol{R}^{n\times m}$, $M(\boldsymbol{\rho}) \in \boldsymbol{R}^{n\times s}$ are the linear parameter varying matrices of the model. $x(t) \in \boldsymbol{R}^n$, $(t) \in \boldsymbol{R}^m$, $f_i(t) \in \boldsymbol{R}^s$, $\xi(\boldsymbol{\rho}, x, t) \in \boldsymbol{R}^k$, and $y(t), \vartheta(t) \in \boldsymbol{R}^p$, are model states, control input signal, faults of actuators, model uncertainty, and measurement noises, respectively. s and p are the lengths of fault and output signal. It is supposed that s is smaller than p ($s < p$). $\boldsymbol{\rho}$ is the varying parameter vector and is measured or estimated. C is an LTI and full-rank matrix. Also, for Lyapunov stability [32], $\xi(\boldsymbol{\rho}, x, t)$ and $\dot{\xi}(\boldsymbol{\rho}, x, t)$ are assumed to be bounded.

Assumption 1. The actuator fault matrix might be parameter varying ($M(\boldsymbol{\rho})$). It is assumed $M(\boldsymbol{\rho})$ is made up of a parameter invariant matrix (M_{inv}) multiplied by a nonsingular parameter varying matrix ($M_{var}(\boldsymbol{\rho})$) in a way that

$$M(\boldsymbol{\rho}) = M_{inv}M_{var}(\boldsymbol{\rho}) \tag{9}$$

where, $M_{inv} \in \boldsymbol{R}^{n\times s}$ and $M_{var}(\boldsymbol{\rho}) \in \boldsymbol{R}^{s\times s}$. Defining a new variable $\sigma(\boldsymbol{\rho}, t) = M_{var}(\boldsymbol{\rho})f_i(t)$, (8) is rewritten in the form of

$$\begin{aligned} \dot{x}(t) &= A(\boldsymbol{\rho})x(t) + B(\boldsymbol{\rho})u(t) \\ &\quad + M_{inv}\,\sigma(\boldsymbol{\rho}, t) \\ &\quad + Q\xi(\boldsymbol{\rho}, x, t) \\ y(t) &= Cx(t) + \vartheta(t) \end{aligned} \tag{10}$$

$\sigma(\boldsymbol{\rho}, t)$ is the new fault vector which will be converted to the actual fault vector ($f_i(t)$) after being estimated. The new fault signal is bounded due to the Lyapunov stability proof [32].

Assumption 2. $\vartheta(t)$ presents the corruption of sensor measurements and is assumed

$$\vartheta(s) = D(s)\varphi(s) \tag{11}$$

$$D(s) = \frac{a_f}{s + a_f} \tag{12}$$

$D(s)$ is a stable transfer function and $\varphi(t)$ is an unknown but bounded signal [30]. Using this assumption, the effect of output noises on estimations is optimized (this will be discussed later). Then, substituting (11) into (12) yields

$$\dot{\vartheta}(t) = -a_f\vartheta(t) + a_f\varphi(t) \tag{13}$$

Assumption 3. $rank(CM) = s$. This condition determines whether the effect of the fault signal is observable in outputs or not. This is a necessary condition for the fault estimation method presented by Tan and Edwards [33].

B. Second-order LPV Sliding Mode Observer

The LPV sliding mode observer is in the form of

$$\begin{aligned} \dot{\hat{x}}(t) &= A(\boldsymbol{\rho})\hat{x}(t) + B(\boldsymbol{\rho})u(t) \\ &\quad + H_{eq}(\boldsymbol{\rho})e_y(t) \\ &\quad + H_{sw}w(t) \\ \hat{y}(t) &= C\hat{x}(t) \end{aligned} \tag{14}$$

where, $H_{eq}(\boldsymbol{\rho})$ and H_{sw} are observer design matrices and $w(t)$ represents discontinuous output error injection to induce a sliding motion [33]. $e(t)$ and $e_y(t)$ as state estimation error and output estimation error are expressed as

$$e(t) = \hat{x}(t) - x(t) \tag{15}$$

$$e_y(t) = \hat{y}(t) - y(t) = Ce(t) - \vartheta(t) \tag{16}$$

The design steps are expressed in the following. First, the system is transformed in a way that the states are classified into measured states (outputs) and unmeasured states [34]. It is proved that the measured states are estimated in a finite time defining the sliding surface as $S = \{e(t) \in R^n : e_y(t) = 0\}$ [34]. Then, with the appropriate choice of parameters, unmeasured states are estimated asymptotically. Finally, the faults are reconstructed using $w(t)$.

As stated before, sliding mode observer gains are divided into an equivalent gain for linear terms and switching motion gain for nonlinear terms. The equivalent gain ($H_{eq}(\boldsymbol{\rho})$) and its corresponding linear signal are existed to force the incidence of the sliding motion. Such an action is called the reaching phase [27].

Furthermore, the switching gain (H_{sw}) and its corresponding nonlinear signal ($w(t)$) are responsible for the maintenance of sliding motion which is called the sliding phase.

There exists a coordinate-transformation $x_f(t) \rightarrow T_f x(t)$ which changes the output matrix to the form of $C_f = [0_{p\times(n-p)} \; T_{p\times p}]$ in which T is an orthogonal nonsingular matrix.

Here, the index 'f' refers to the system of $x_f(t)$. Also, for an invertible square matrix M_0, the fault matrix becomes in the form of (17).

$$M_{inv,f} = \begin{bmatrix} 0_{(n-p)\times s} \\ 0_{(p-s)\times s} \\ M_{0_{s\times s}} \end{bmatrix} \tag{17}$$

Then, the following structure is obtained after the first transformation.

$$y_f(t) = [0 \;\; T]\begin{bmatrix} x_{1,f} \\ x_{2,f} \end{bmatrix} + \vartheta(t) \tag{18}$$

$$A_f(\boldsymbol{\rho}) = \begin{bmatrix} A_{11,f} & A_{12,f} \\ A_{21,f} & A_{22,f} \end{bmatrix} \tag{19}$$

$$Q_f = \begin{bmatrix} Q_{1,f} \\ Q_{2,f} \end{bmatrix} \tag{20}$$

Rewriting (8) and using the structures of (17)-(20) yields

$$\begin{aligned} \begin{bmatrix} \dot{e}_{1,f} \\ \dot{e}_{2,f} \end{bmatrix} = A_f \begin{bmatrix} e_{1,f} \\ e_{2,f} \end{bmatrix} &- Q_f \xi(\boldsymbol{\rho}, x, t) \\ &- H_{eq,f}(\boldsymbol{\rho}) e_y(t) \\ &+ H_{sw,f} w(t) \\ &- \begin{bmatrix} 0_{(n-s)\times s} \\ M_{0_{s\times s}} \end{bmatrix} \sigma(\boldsymbol{\rho}, t) \end{aligned} \tag{21}$$

Using (8) and (21)

$$e_y(t) = T e_{2,f} - \vartheta(t)$$

Thus, if the sliding motion takes place, from the definition $e_y(t) = 0$ and then $T e_{2,f} = \vartheta(t)$. Using (21) and regarding T as an orthogonal matrix gives:

$$\begin{aligned} \dot{e}_{1,f}(t) &= A_{11,f} + A_{12,f} T^T \vartheta(t) - L T^T w_{eq}(t) \\ &\quad - Q_{1,f} \xi(\boldsymbol{\rho}, x, t) \end{aligned} \tag{22}$$

$$\begin{aligned} 0 &= T A_{21} e_{1,f}(t) - T Q_{2,f} \xi(\boldsymbol{\rho}, x, t) \\ &\quad + T A_{22} T^T \vartheta(t) - \dot{\vartheta}(t) \\ &\quad + w_{eq}(t) - T \begin{bmatrix} 0_{(p-s)\times s} \\ M_{0_{s\times s}} \end{bmatrix} \sigma(\boldsymbol{\rho}, t) \end{aligned} \tag{23}$$

$w_{eq}(t)$ is the equivalent output error injection i.e. the same as $w(t)$ after the sliding motion. As a definition, for a design matrix $Y \in \boldsymbol{R}^{s\times(p-s)}$ and the structure of $W = [\mathrm{Y} \quad M_0^{-1}]$ the new fault signal is reconstructed as

$$\hat{\sigma}(\boldsymbol{\rho}, t) = W T^T w_{eq}(t) \tag{24}$$

In the system of (21), the LTI observer gain is considered in the form of

$$H_{sw,f} = \begin{bmatrix} -L T^T \\ T^T \end{bmatrix} \tag{25}$$

L is the design matrix and is of the form

$$L = [Z \;\; 0_{(n-p)\times s}] \text{ and } Z \in \boldsymbol{R}^{(n-p)\times(p-s)} \tag{26}$$

Z improves the sliding motion incidence and is synthesized by solving some matrix inequalities (it will be discussed later). Joining measurement noises signal and $e_{1,f}(t)$ together as a new state vector, an assembled state-space is obtained.

$$\begin{aligned} e_a(t) &= A_a(\boldsymbol{\rho}) e_a(t) + B_a(\boldsymbol{\rho}) \xi_a(t) \\ \hat{\sigma}(\boldsymbol{\rho}, t) - \sigma(\boldsymbol{\rho}, t) &= C_a e_a(t) + F_a \xi_a(t) \end{aligned} \tag{27}$$

where,

$$\begin{aligned} e_a^T(t) &= \left[T^T \vartheta(t) \quad e_{1,f}(t)\right]^T, \\ \xi_a^T(t) &= [\xi(t) \quad T^T \varphi(t)]^T \\ A_a(\boldsymbol{\rho}) &= \begin{bmatrix} -a_f I_p & 0_{p\times(n-p)} \\ A_{12}(\boldsymbol{\rho}) + L A_{22}(\boldsymbol{\rho}) + a_f L & A_{11} + L A_{21}(\boldsymbol{\rho}) \end{bmatrix} \end{aligned} \tag{28}$$

$$B_a(\boldsymbol{\rho}) = \begin{bmatrix} 0_{p\times(n-p)} & -a_f I_p \\ -Q_{1,f} - L Q_{2,f} & -a_f L \end{bmatrix} \tag{29}$$

$$\begin{aligned} C_a(\boldsymbol{\rho}) \\ = [-(W A_{22}(\boldsymbol{\rho}) + a_f W) \quad -W A_{21}(\boldsymbol{\rho})] \end{aligned} \tag{30}$$

$$F_a = [W Q_{2,f} \quad a_f W] \tag{31}$$

The effect of uncertainty and measurement noises are minimized if there exist positive definite and symmetric matrices ${P_{af}}_{p\times p}$ and ${P_{11}}_{(n-p)\times(n-p)}$ such that the following matrix inequalities hold

$$\boldsymbol{X}(\boldsymbol{\rho}) = \begin{bmatrix} P_1 A_a + {A_a}^T P_1 & P_1 B_a \Delta & C_a^T \\ (B_a)^T P_1 & -\gamma I & (F_a)^T \\ C_a & F_a \Delta & -\gamma I \end{bmatrix} < 0 \tag{32}$$

$$P_1 = \begin{bmatrix} P_{11} & 0 \\ 0 & P_{af} \end{bmatrix} > 0 \tag{33}$$

where, $\Gamma > 0$ means Γ is a positive definite matrix; then, using bounded real lemma $\|\hat{\sigma}(\boldsymbol{\rho},t) - \sigma(\boldsymbol{\rho},t)\| < \gamma\|\xi_a(\boldsymbol{\rho},t)\|$. Also,

Remark 1. It should be mentioned that there exist parameter varying terms in the matrix inequality (32) which make it confusing to solve the matrix inequality to determine a unique minimized γ. Therefore, we are unable to obtain the second transformation and the design matrices and the range of variation of $\boldsymbol{\rho}$ has to be considered. As a result, the effects of uncertainty and measurement noises are almost minimized.

Once L is obtained, the observer gain $H_{sw,f}$ is calculated and reverted to a system of (10) using

$$H_{sw} = T_f^{-1} \times H_{sw,f} \tag{34}$$

After obtaining the design matrix L, a second transformation is applied to the system of (21) where C_f is reformed into $C_s = [0_{p\times(n-p)} \;\; I_p]$. 's' represents second coordinate transformation.

$$\begin{bmatrix} x_{1,s} \\ x_{2,s} \end{bmatrix} = T_s \begin{bmatrix} x_{1,f} \\ x_{2,f} \end{bmatrix}$$
$$\text{where } T_s = \begin{bmatrix} I_{(n-p)\times(n-p)} & L \\ 0_{p\times(n-p)} & T \end{bmatrix} \tag{35}$$

$$A_s(\boldsymbol{\rho}) = \begin{bmatrix} A_{11,s} & A_{12,s} \\ A_{21,s} & A_{22,s} \end{bmatrix} \tag{36}$$

$H_{eq}(\boldsymbol{\rho})$ in the second coordination is obtained online after the calculation of L in a parameter varying structure of

$$H_{eq,s}(\boldsymbol{\rho}) = \begin{bmatrix} A_{12,s}(\boldsymbol{\rho}) \\ A_{22,s}(\boldsymbol{\rho}) + k_2 I_p \end{bmatrix} \tag{37}$$

$H_{eq,s}(\boldsymbol{\rho})$ is reverted to the main coordinates (14) by

$$H_{eq}(\boldsymbol{\rho}) = T_f^{-1} \times T_s^{-1} \times H_{eq,s}(\boldsymbol{\rho}) \tag{38}$$

The notation of j'th component of a vector $\vec{V}$ is defined as an index, e.g. V_j. Then, the equivalent output injection signal is calculated cell by cell separately in

$$w_j(t) = -k_1 sign\left(e_{y,j}(t)\right)\left|e_{y,j}(t)\right|^{\frac{1}{2}} + z_j(t) \tag{39}$$

$$\dot{z}_j(t) = -k_3 sign\left(e_{y,j}(t)\right) - k_4 e_{y,j}(t) \tag{40}$$

for *j=1,2,...,p*

k_1, k_2, k_3, k_4 are design parameters in satisfying inequalities below. By choosing proper values of scalars k_1, k_2, k_3, k_4, second-order sliding motion takes place in a finite time and the fault reconstruction process begins where proof by the Lyapunov method is explained in [35].

$$k_1 > 2\sqrt{\epsilon}$$
$$k_2 > 0 \tag{41}$$
$$k_3 > \epsilon$$
$$k_4 > \frac{k_2^2[(k_1)^3 + 1.25(k_1)^2 + 2.5(k_3 - \epsilon)]}{k_1(k_3 - \epsilon)}$$

ϵ is the bound of fault incidence rate or $\left|\dot{f}_i(t)\right| < \epsilon$. Substituting (40) into (39), the output injection signal is obtained by

$$w_j(t) = -k_1 sign\left(e_{y,j}(t)\right)\left|e_{y,j}(t)\right|^{\frac{1}{2}} + \int \left[-k_3 sign\left(e_{y,j}(s)\right) - k_4 e_{y,j}(s)\right] ds \tag{42}$$

By substituting (9) into (24), the fault estimation signal becomes

$$\hat{f}_i(t) = M_{var}^{-1}(\boldsymbol{\rho})\hat{\sigma}(\boldsymbol{\rho},t) = M_{var}^{-1}(\boldsymbol{\rho})WT^T w(t) \tag{43}$$

It should be mentioned that fault reconstruction in (43) is obtainable if only the sliding motion takes place.

Remark 2. The estimation of the new fault signal is enhanced by exploiting a low-pass filter in the form of

$$F(s) = \frac{b}{s+b} \tag{44}$$

Such a filter lowers the high frequency of measurement noises to enhance the new fault estimation signal. Filter reduces the amplitude of noises and results in a smoother estimation signal.

Remark 3. The method explained in Section 3 does not require any redundant instruments. Usually, wind turbine sensors consist of three pitch angles, generator and rotor speed, generator torque, and effective wind speed [16]. Using the filtered sensors' data and a microcomputer, the proposed FDI algorithm could be implemented and states and pitch faults are calculated.

Observability of the wind turbine model is inspected which is baffling due to the LPV description of wind turbine plant (Section 5) [36], where using Simulink, we watched the rank of LPV observability matrix online. For all the wind turbine operating regions $rank(\boldsymbol{O}_{LPV}) = 6$; therefore, the system is observable and the states can be estimated utilizing a proper observer.

Pitch Actuator Fault Model

It is assumed that an identical performance and fault occur in all the pitch systems, and we only look through one system.

A second-order transfer function is assumed for each of the pitch actuators. Thus, the pitch angle and pitch rate are regarded as the system states.

The matching condition mentioned in assumption 3 does not hold unless a change of variables in dynamic equations of the pitch system is performed.

$$\begin{bmatrix}\beta(t)\\ \dot{\beta}'(t)\end{bmatrix} \to \bar{T}\begin{bmatrix}\beta(t)\\ \dot{\beta}(t)\end{bmatrix} \quad (45)$$

where, $\bar{T} = \begin{bmatrix}1 & 0\\ 0 & \frac{1}{\omega_n^2(t)}\end{bmatrix}$ and the pitch system equations are transformed to

$$\begin{bmatrix}\dot{\beta}(t)\\ \ddot{\beta}'(t)\end{bmatrix} = \begin{bmatrix}0 & \omega_n^2(t)\\ -1 & -2\zeta(t)\omega_n(t)\end{bmatrix}\begin{bmatrix}\beta(t)\\ \dot{\beta}'(t)\end{bmatrix} \quad (46)$$

Therefore, the assumption of $rank(CM_{inv}) = 1 = s \le p = 1$ still holds.

Hydraulic leakage affects the pitch actuator properties such as the natural frequency and damping ratio of each actuator. The system properties are $\omega_{n,h}$ and ζ_h as healthy and $\omega_{n,f}$ and ζ_f as a faulty situation. Then, considering the fault as changing properties in a linear fraction of both healthy and faulty mode, the incidence of the fault is modeled using two varying parameters $\theta_1$and θ_2. $\theta_1 = \theta_2 = 0$ means no fault in the system and $\theta_1 = \theta_2 = 1$ indicates a totally faulty situation.

$$\begin{aligned}\omega_n^2(t) &= \theta_1(t)\omega_{n,f}^2 + (1-\theta_1(t))\omega_{n,h}^2\\ &= \omega_{n,h}^2 + \theta_1(t)\left[\omega_{n,f}^2 - \omega_{n,h}^2\right]\end{aligned} \quad (47)$$

$$\begin{aligned}-2\zeta(t)\omega_n(t) &= -2\zeta_f\omega_{n,f}\theta_2(t)\\ &\quad + \left(1-\theta_2(t)\right)(-2\zeta_h\omega_{n,h})\\ &= -2\zeta_h\omega_{n,h}\\ &\quad + \theta_2(t)\left[-2\zeta_f\omega_{n,f}\right.\\ &\quad \left. + 2\zeta_h\omega_{n,h}\right]\end{aligned} \quad (48)$$

It is assumed that the set of $\{\omega_{n,h}, \zeta_h\}$ or the set of $\{\omega_{n,f}, \zeta_f\}$ occur, simultaneously. When the pitch system performance is normal, its properties are in a healthy situation. Malfunctioning of the pitch system means a faulty situation for both properties. Thus, $\theta_1(t) \approx \theta_2(t)$. Substituting (47) and (48) into (46), yields

$$\begin{aligned}&\begin{bmatrix}0 & \omega_n^2(t)\\ -1 & -2\zeta(t)\omega_n(t)\end{bmatrix}\\ &= \begin{bmatrix}0 & \omega_{n,h}^2 + \theta_1(t)\left(\omega_{n,f}^2 - \omega_{n,h}^2\right)\\ -1 & -2\zeta_h\omega_{n,h} + \theta_1(t)\left(-2\zeta_f\omega_{n,f} + 2\zeta_h\omega_{n}\right.\end{bmatrix}\\ &= \begin{bmatrix}0 & \omega_{n,h}^2\\ -1 & -2\zeta_h\omega_{n,h}\end{bmatrix}\\ &+ \begin{bmatrix}0 & \theta_1(t)\left(\omega_{n,f}^2 - \omega_{n,h}^2\right)\\ 0 & \theta_1(t)\left(-2\zeta_f\omega_{n,f} + 2\zeta_h\omega_{n,h}\right)\end{bmatrix}\end{aligned} \quad (49)$$

Multiplying (50) with the states gives,

$$\begin{aligned}&\begin{bmatrix}0 & \theta_1(t)\left(\omega_{n,f}^2 - \omega_{n,h}^2\right)\\ 0 & \theta_1(t)\left(-2\zeta_f\omega_{n,f} + 2\zeta_h\omega_{n,h}\right)\end{bmatrix}\begin{bmatrix}\beta(t)\\ \dot{\beta}'(t)\end{bmatrix}\\ &= \begin{bmatrix}\omega_{n,f}^2 - \omega_{n,h}^2\\ -2\zeta_f\omega_{n,f} + 2\zeta_h\omega_{n,h}\end{bmatrix}\dot{\beta}'(t)\theta_1(t)\\ &= M_{inv}M_{var}(\boldsymbol{\rho})f_i(t)\end{aligned} \quad (50)$$

where, $M_{inv} = \begin{bmatrix}\omega_{n,f}^2 - \omega_{n,h}^2\\ -2\zeta_f\omega_{n,f} + 2\zeta_h\omega_{n,h}\end{bmatrix}$ and $M_{var}(\boldsymbol{\rho}) = \rho_4$, $f_i(t) = \theta_1(t)$. Therefore, the process fault is modeled as an actuator additive fault in (50).

Wind Turbine LPV Description

Tables may place within the texts or just before the figures. All quantities in tables should be accompanied by their units. Table footnotes should be indicated by letters a, b, c, etc. The states of the wind turbine model are rotor rotational speed, generator speed, torsion angle of the drive-train, generator torque, pitch angle, and pitch angle rate. One of the purposes of the first transformation is reshaping the output matrix. Therefore, we rearrange the order of the states in a way that the specific structure takes place. The state vector is defined as

$$\begin{aligned}&x(t)\\ &= \left[\dot{\beta}'(t) \quad \theta(t) \quad \omega_r(t) \quad \omega_g(t) \quad T_g(t) \quad \beta(t)\right.\end{aligned} \quad (51)$$

Among the considered states in the model, the drive-train equation is severely nonlinear. Such a nonlinear differential equation can be linearized and expressed in a linear parameter varying manner where the model matrices change with a varying parameter. The drive-train equation is shown in (52).

$$\begin{aligned}\dot{\omega}_r(t) &= \frac{1}{J_r}T_a(\omega_r, \beta, V_w, t) - \frac{K_{dt}}{J_r}\theta(t)\\ &\quad - \frac{B_{dt} + B_r}{J_r}\omega_r(t)\\ &\quad + \frac{B_{dt}}{J_r}\omega_g(t)\end{aligned} \quad (52)$$

The nonlinear term is $T_a(\omega_r, \beta, V_w, t)$ which is the aerodynamic torque exerted by the wind turbine and estimated in the form $T_a(\omega_r, \beta, V_w, t) = \frac{1}{2}\rho_{air}\pi R^3 C_q(\omega_r, \beta, V_w)V_w^2$. C_q is a torque coefficient table and consists of aerodynamic experimental data. Using surface fitting by the well-known software MATLAB, a fifth-degree (quintic) polynomial is derived in which ω_r, β, V_w are the variables. The interpolated form of $\frac{1}{J_r}T_a(\omega_r, \beta, V_w, t)$ becomes

$$\begin{aligned}T_a(\omega_r, \beta, V_w, t)/J_r &= p_1V_w\omega_r + p_2\omega_r^2\\ &\quad + p_3\frac{\omega_r^3}{V_w} + p_4\frac{\omega_r^4}{V_w^2} + p_5\frac{\omega_r^5}{V_w^3}\\ &\quad + p_6V_w\omega_r\beta + p_7V_w\omega_r\beta^2\\ &\quad + p_8V_w\omega_r\beta^3 + p_9V_w\omega_r\beta^4\\ &\quad + p_{10}V_w^2\beta + p_{11}\omega_r^2\beta\\ &\quad + p_{12}V_w^2\beta^2 + p_{13}V_w^2\beta^3\\ &\quad + p_{14}V_w^2\beta^4 + p_{15}V_w^2\beta^5\\ &\quad + p_{16}\omega_r^2\beta^2 + p_{17}\omega_r^2\beta^3\\ &\quad + p_{18}\frac{\omega_r^3\beta}{V_w} + p_{19}\frac{\omega_r^3\beta^2}{V_w}\\ &\quad + p_{20}\frac{\omega_r^3\beta}{V_w} + p_{21}V_w^2\end{aligned} \quad (53)$$

To validate the accuracy of the model, the parameters of the benchmark and presented model are compared. Fig. 2 demonstrates real data points (colored surface) and some sampled data from the LPV model (black points).

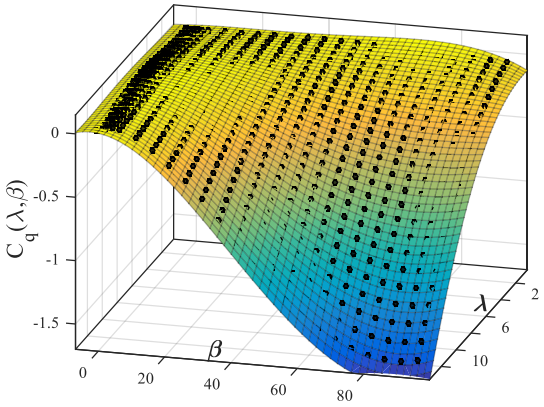

Fig. 2: Torque aerodynamic coefficient (10) (colored surface) and sample points from the proposed model (black points).

The black points approximately coincide with the real data surface showing the validity of the model. The varying parameters are capsulated in $\boldsymbol{\rho} = [V_w, \omega_r, \beta, \dot{\beta}']^T$. Then, a new structure is obtained by rearranging (53). Table 2 consists of the LPV coefficients.

Table 2: Coefficients of the wind turbine LPV model

$p_1 = 2.13e-5$	$p_2 = -8.18e-3$	$p_3 = -3.92e-5$
$p_4 = 2.89e-1$	$p_5 = -3.70e-7$	$p_6 = 2.17e-10$
$p_7 = -1.10e-11$	$p_8 = 2.47e-13$	$p_9 = -2.63$
$p_{10} = 9.26$	$p_{11} = -11.42$	$p_{12} = -1.27e-4$
$p_{13} = 8.89e-7$	$p_{14} = 1.44e-2$	$p_{15} = -3.34e-2$
$p_{16} = -3.15e-4$	$p_{17} = 1.31e-5$	$p_{18} = -2.36e-7$
$p_{19} = 1.53e-7$	$p_{20} = -1.2e-9$	

$$
\begin{aligned}
&T_a(\omega_r, \beta, V_w, t)/J_r \\
&\quad = \Big[p_1\rho_1 + p_2\rho_2 + p_3\frac{\rho_2^2}{\rho_1} + p_4\frac{\rho_2^3}{\rho_1^2} \\
&\quad + p_5\frac{\rho_2^4}{\rho_1^3} + p_6\rho_1\rho_3 + p_7\rho_1{\rho_3}^2 \\
&\quad + p_8\rho_1{\rho_3}^3 + p_9\rho_1{\rho_3}^4\Big]\omega_r \\
&\quad + \Big[p_{10}V_w^2\beta + p_{11}\rho_2^2 + p_{12}\rho_1^2\rho_3 \\
&\quad + p_{13}\rho_1^2{\rho_3}^2 + p_{14}\rho_1^2{\rho_3}^3 + p_{15}\rho_1^2{\rho_3}^4 \\
&\quad + p_{16}\rho_2^2\rho_3 + p_{17}\rho_2^2{\rho_3}^2 + p_{18}\frac{\rho_2^3}{\rho_1} \\
&\quad + p_{19}\frac{\rho_2^3\rho_3}{\rho_1} + p_{20}\frac{\rho_2^3}{\rho_1}\Big]\beta + p_{21}V_w^2 \\
&\quad = \Delta A_{3,3}\omega_r + \Delta A_{3,6}\beta + p_{21}V_w^2
\end{aligned}
\tag{54}
$$

Substituting into (52) results in

$$
\begin{aligned}
\dot{\omega}_r(t) = &-\frac{K_{dt}}{J_r}\theta(t) - \frac{B_{dt}+B_r}{J_r}\omega_r(t) \\
&+ \frac{B_{dt}}{J_r}\omega_g(t) \\
&+ \Delta A_{3,3}(\boldsymbol{\rho})\omega_r(t) \\
&+ \Delta A_{3,6}(\boldsymbol{\rho})\beta(t) + p_{21}V_w^2
\end{aligned}
\tag{55}
$$

We are unable to merge the last term of the (55) in the system matrix and it is considered as model uncertainty. The LPV description of the model is expressed in

$$
\begin{aligned}
&A(\boldsymbol{\rho}) \\
&= \begin{bmatrix}
-2\zeta_h\omega_{n,h} & 0 & 0 & 0 & 0 & -1 \\
0 & 0 & 1 & -\frac{1}{N_g} & 0 & 0 \\
0 & -\frac{K_{dt}}{J_r} & a_{33}(\boldsymbol{\rho}) & \frac{B_{dt}}{N_g J_r} & 0 & a_{36}(\boldsymbol{\rho}) \\
0 & \frac{\eta_{dt}K_{dt}}{N_g J_g} & \frac{\eta_{dt}B_{dt}}{N_g J_g} & a_{44} & -\frac{1}{J_g} & 0 \\
0 & 0 & 0 & 0 & -\alpha_{gc} & 0 \\
\omega_{n,h}^2 & 0 & 0 & 0 & 0 & 0
\end{bmatrix} \\
&B = \begin{bmatrix} 0 & 0 & 0 & 0 & \alpha_{gc} & 0 \\ 1 & 0 & 0 & 0 & 0 & 0 \end{bmatrix}^T, \\
&C = \begin{bmatrix} 0 & 0 & 1 & 0 & 0 & 0 \\ 0 & 0 & 0 & 1 & 0 & 0 \\ 0 & 0 & 0 & 0 & 1 & 0 \\ 0 & 0 & 0 & 0 & 0 & 1 \end{bmatrix}, \\
&Q = [0 \quad 0 \quad 1 \quad 0 \quad 0 \quad 0]^T, \\
&M_{inv} = [m_1 \quad 0 \quad 0 \quad 0 \quad 0 \quad m_6]^T, \\
&M_{var}(\boldsymbol{\rho}) = \rho_4, \; u(t) = [\tau_{g,r}(t) \quad \beta_r(t)]^T, f_i(t) = \theta_1(t)
\end{aligned}
\tag{56}
$$

A summary of the wind turbine fault reconstruction and observation is illustrated in Fig. 3.

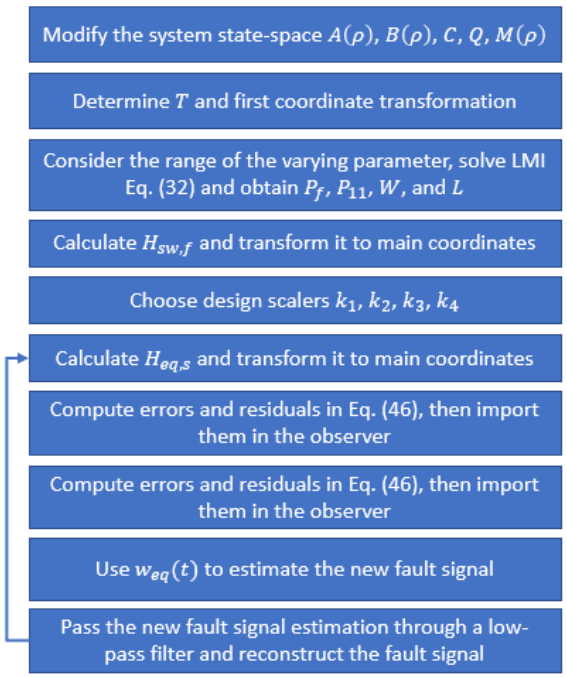

Fig. 3: Design algorithm flowchart for wind turbine fault reconstruction.

Results and Discussion

In this section, reconstruction of pitch actuator fault is investigated. The observability of the proposed model has been checked in Section 3.3. The observability matrix (51) is full-rank during the operation which means the model is observable even by the time-varying nature of $\boldsymbol{\rho}$. Considering the structure in (17), $T = I_4$ and

$$T_f = \begin{bmatrix} 46.7 & 0 & 0 & 0 & 0 & 3 \\ 15.6 & 1 & 0 & 0 & 0 & 1 \\ 0 & 0 & 1 & 0 & 0 & 0 \\ 0 & 0 & 0 & 1 & 0 & 0 \\ 0 & 0 & 0 & 0 & 1 & 0 \\ 0 & 0 & 0 & 0 & 0 & 1 \end{bmatrix}$$

Then, solving matrix inequality (32) gives P_f, P_{11}, L and W. Once L is calculated, the first observer gain $H_{eq}(\boldsymbol{\rho})$ is built in the structure of (41). The second transformation is then possible substituting L in (39). The fault is reconstructed substituting W and T in (47).

$$P_{af} = \begin{bmatrix} 3.41 & -0.0019 & 3.35 & 1.61e-8 \\ -7.854 & -4.31e-10 & 3.35 & -10.82 \\ 3.35 & 3.35 & 5.12e-4 & -2.88e-2 \\ 1.61e-8 & -2.88e-2 & -7.44e-9 & 7.11 \end{bmatrix}$$

$$L = \begin{bmatrix} 0.0011 & -1.86e-5 & 5.22e-24 & 0 \\ -0.0075 & -2.48e-5 & 3.26e-24 & 0 \end{bmatrix}$$

$$W = [8.81e-5 \quad -1.06e-7 \quad 0 \quad -8.95e-3]$$

$$P_{11} = \begin{bmatrix} 17.2 & -35.9 \\ -35.9 & 112.8 \end{bmatrix}$$

$$k_1 = 10, k_2 = 1, k_3 = 50, k_4 = 100, a_f = 50$$

Wind speed, as stochastic input data, has been manipulated using a stochastic input profile gathered from the actual wind speed measurements of a wind park [37] An average of 15 m/s has been chosen for wind speed which is included in region 3 of operation regions.

A high-slope ramp (nearly unit step) between 8th to 14th seconds is considered as an actuator fault in the pitch system caused by hydraulic leakage. Hydraulic leakage is an incipient and fast decaying fault [7]. The range and the rate of such a fault are illustrated in Table 1. To emphasize the paper methodology i.e. robust LPV fault reconstruction using second-order sliding mode observers, a different fault scenario is inspected. To exhibit the rapid and precise fault recognition and reconstruction, it is supposed that an abrupt fault takes place faster than 1/(100 seconds) (according to Table 1) in the simulation.

Fig. 4 shows the reconstruction of the LPV fault indicator in the presence of model uncertainty and measurement noise during 6 seconds. A step is considered as the fault indicator θ_1. Also, the estimation of pitch system properties (natural frequency and damping ratio) are illustrated in Fig. 4.

As shown in Fig. 4, once an actuator fault occurs, it is reconstructed accurately and immediately. The effects of noises and uncertainty have been minimized in (32). However, the fault estimation signal conveys noise between the 8th to 14th seconds. The estimation of the new fault signal in (24) is enhanced by exploiting a low-pass filter in the form of

$$F(s) = \frac{10}{s+10} \tag{60}$$

As mentioned, the new fault signal in (10) is passed through a low-pass filter $F(s)$ in order to become smoother in (44). The measurement noise in all of the sensors appears as fluctuations. The measurement noises' powers are chosen as $\|\varphi_{\omega_r}\| = 10^{-5}$, $\|\varphi_{\omega_g}\| = 10^{-1}$, $\|\varphi_{\tau_g}\| = 10^{+3}$, and $\|\varphi_{\beta}\| = 10^{-4}$. It should be noted that the robustness of the proposed observer is not disturbed by the amplitude of the noises with known bounds. In addition, all the measurements could be properly filtered to avoid the harmful effects of the noises in state estimation.

Figs. 5 & 6 illustrate the performance of second-order sliding mode observers in the presence of pitch actuator fault. The estimation signals converge to the system states in at most 2.5 seconds with less than 2.48 percent estimation error in generator speed.

Rahnavard et al. [22] used an LTI first-order sliding mode observer to reconstruct wind turbine faults. Compared with this paper, both methods are fast and accurate and also overcome the output noises' effects. But, the proposed LPV method covers all the wind turbine operating regions and no linearization approximations are required at the cost of heavier computations. While in [22], the nonlinear equations are linearized around an operating point. It requires gain-scheduling and switching among the models which reduces the robustness and model-accuracy of the method.

Sloth et al. [17], used robust theory for LPV active-fault-tolerant control of a benchmark model, similar to this paper. The LPV model in [17], contains linearizing the aerodynamic torque around a floating trajectory. The LPV model of the current paper uses a quintic multi-variable polynomial instead of linearization which improves the accuracy.

A time-invariant sliding mode observer (with the same procedure for designing observer gains) is carried out for a nonlinear model in which the aerodynamic torque is regarded as the uncertainty ($\xi_{NL} = T_a/J_r$). It should be mentioned that $\xi_{LPV} = p_{21}V_w^2$ from (55) is considered as the uncertainty signal, exerting the proposed LPV model.

Fig. 7 illustrates the comparison between the fault reconstruction performance of the nonlinear model (in which the aerodynamic torque is regarded as an uncertainty) and the LPV model of a wind turbine from Section 5. As expected, the LPV model provides a more

accurate estimation of the actuator faults using the same filters (60).

As an average value, the amplitude of fluctuations of fault reconstruction in the nonlinear model is approximately 11.5 times larger than fluctuations of fault reconstruction in the LPV model.

In addition, the mean value of fault reconstruction of the nonlinear model is biased about 3 percent before fault occurrence which demonstrates the weaker performance of the observer, affected by large uncertainty ($\xi_{NL} = T_a/J_r$).

It arises from the severe nonlinearity of aerodynamic torque which is handled using LPV methods. In this case, the magnitude of uncertainty in (58) is much less than that in the nonlinear model i.e. $\|\xi_{LPV}\| = 0.0288\, rad/s^2$ in comparison with $\|\xi_{NL}\| = 0.8979\, rad/s^2$. In addition, the observer LPV gain is calculated in an adaptive manner (38).

Conclusion

The application of SMO on a wind turbine system that contains a parameter varying model is investigated. The results of this paper show that the sliding mode fault reconstruction method is applicable for LPV systems. It is interesting to note that the severity of the pitch hydraulic pump is estimated while the model parameters are varying, sensors are faulty, and some parameters are uncertain.

The LPV model of a wind turbine is derived by surface interpolation and fitting a quintic polynomial for the aerodynamic torque coefficient. The LPV model predicts the real behavior of the system with the highest error of 3.2 percent.

The robustness of the estimation and reconstruction scheme is another merit of the proposed SMO as shown in the results. Wind speed range is considered from 14 m/s to 16 m/s and it is regarded as a stochastic input exerting aerodynamic torque. Fast and accurate fault reconstruction happens in 0.6 seconds with less than one percent error.

Compared to the previous works, the proposed observer performance is less affected by the pitch actuator fault, and the fault severity is estimated in 2.5 seconds with an error smaller than 2.48 percent. The LPV observer presented in this work covers both of the wind turbine operating regions which are more appropriate for large-scale applications.

As a prospective, the proposed method will be applied to a real large wind turbine to assess its performance. In addition, the tuning mechanism of the design parameters of the proposed observer can be determined by using optimization methods such as genetic algorithm which results in better performance and smaller errors.

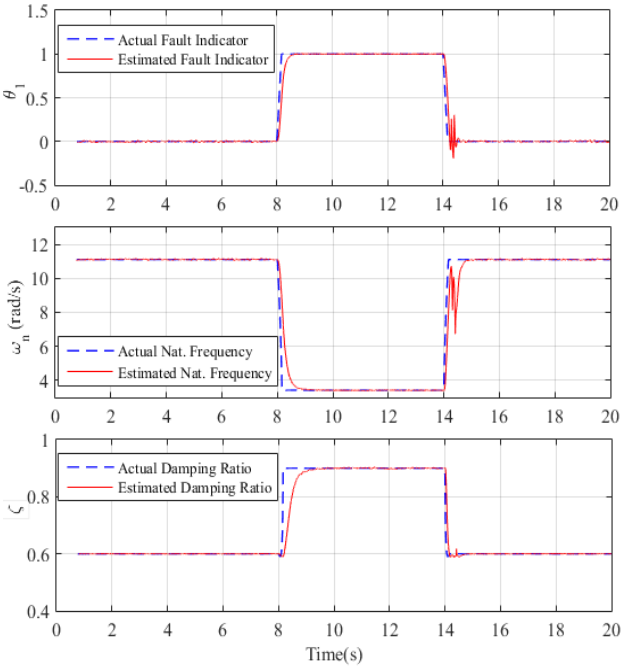

Fig. 4: Fault indicator, natural frequency, and damping ratio of pitch actuator. The Blue (dashed) line is the actual signal and the red (solid) line is the estimation.

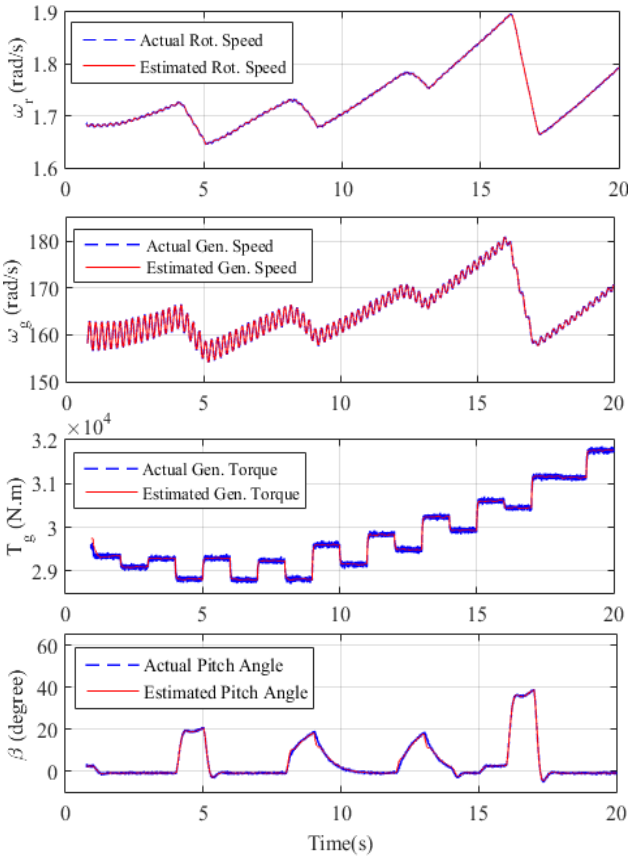

Fig. 5: Measured state estimation (output estimation) using second-order SMO in the presence of pitch actuator.

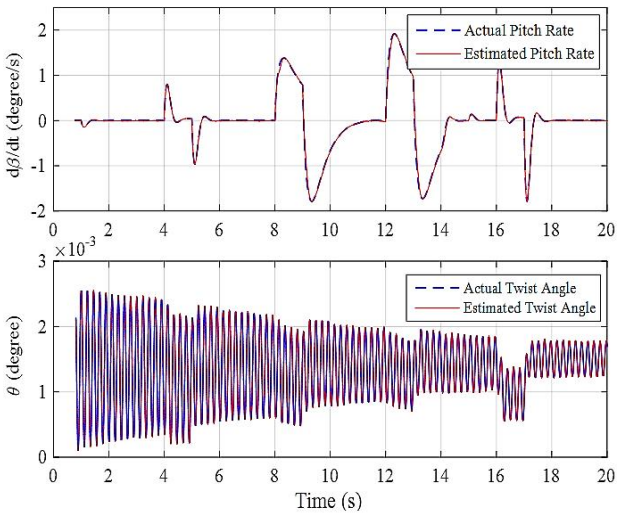

Fig. 6: Unmeasured state estimation using second-order SMO in the presence of pitch actuator fault.

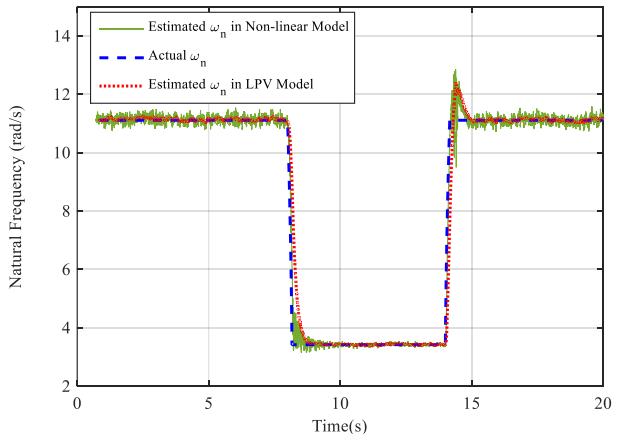

Fig. 7: Comparison of fault reconstruction results in nonlinear model and LPV model.

Author Contributions

M. Mousavi carried out data analysis and simulations. M. Mousavi, and M. Ayati, interpreted the results and wrote the manuscript. M. Mousavi, M. Ayati, M. Hairi-Yazdi, and S. Siahpour revised the manuscript.

Acknowledgment

There is no acknowledgement.

Conflict of Interest

The authors declare no potential conflict of interest regarding the publication of this work. In addition, the ethical issues including plagiarism, informed consent, misconduct, data fabrication and, or falsification, double publication and, or submission, and redundancy have been completely witnessed by the authors.

References

[1] Y. Wentao, G. Hua, X. Shuai, Y. Geng, "Nonlinear individual pitch control of large wind turbines for blade load reduction," in Proc. International Conference on Renewable Power Generation, 2015.

[2] M. Rahnavard, M. Ayati, M. R. Hairi Yazdi, "Robust actuator and sensor fault reconstruction of wind turbine using modified sliding mode observer," Trans. Inst. Meas. Control, 41(6): 1504-1518, 2019.

[3] J. Lan, R. J. Patton, X. Zhu, "Fault-tolerant wind turbine pitch control using adaptive sliding mode estimation," Renewable Energy, 116: 219-231, 2018.

[4] Z. Rafiee, A. Mosahebfard, M. H. Sheikhi, "High-performance ZnO nanowires-based glucose biosensor modified by graphene nanoplates," Mater. Sci. Semicond. Process., 26(10) 115, 2020.

[5] D. Kim, D. Lee, "Hierarchical fault-tolerant control using model predictive control for wind turbine pitch actuator faults," Energies, 12(16): 3097, 2019.

[6] H. Habibi, H. Rahimi Nohooji, I. Howard, "Optimum efficiency control of a wind turbine with unknown desired trajectory and actuator faults," J. Renewable Sustainable Energy, 9(6): 063305, 2017.

[7] T. Esbensen, C. Sloth, S. L. Pedersen, J. M. Holm, T. N. Jensen, M. Philipsen, "Fault diagnosis and fault-tolerant control of wind turbines", Master Thesis, Aalborg University, 2009.

[8] B. Lu, "A review of recent advances in wind turbine condition monitoring and fault diagnosis," in Proc. 2009 IEEE Power Electronics and Machines in Wind Applications: 1-7, 2009.

[9] M. R. Wilkinson, F. Spinato, P. J. Tavner, "Condition monitoring of generators and other subassemblies in wind turbine drive trains," in proc. 2007 IEEE International Symposium on Diagnostics for Electric Machines, Power Electronics and Drives: 388-392, 2007.

[10] S. Khodakaramzadeh, M. Ayati, M. R. Haeri Yazdi, "Fault diagnosis of a permanent magnet synchronous generator wind turbine," J. Electr. Comput. Eng. Innovations (JECEI), 9(2): 143-152, 2021.

[11] S. M. Hosseini, M. Manthouri, "Type 2 adaptive fuzzy control approach applied to variable speed DFIG based wind turbines with MPPT algorithm," Iran. J. Fuzzy Syst., 19(1): 31-45, 2021.

[12] V. Fazlollahi, F. A. Shirazi, M. Taghizadeh, S. Siahpour, "Robust wake steering control design in a wind farm for power optimization using adaptive learning game theory (ALGT) method," International Journal of Control, (Just-accepted): 1 , 2021.

[13] Z. Dehghani Arani, S. A. Taher, M. H. Karimi, M. Rahimi, "Coordinated model predictive DC-Link voltage, current, and electromagnetic torque control of wind turbine with DFIG under grid faults," J. Electr. Comput. Eng. Innovations (JECEI), 8(2): 201-218, 2020.

[14] P. F. Odgaard, J. Stoustrup, M. Kinnaert, "Fault tolerant control of wind turbines – a benchmark model," in Proc. 7th IFAC Symposium on Fault Detection, Supervision and Safety of Technical Processes, 42(8): 155-160, 2009.

[15] H. Badihi, Y. Zhang, H. Hong, "Fuzzy gain-scheduled active fault-tolerant control of a wind turbine," J. Franklin Inst., 351(7): 3677–706, 2014.

[16] Y. Yin, P. Shi, F. Liu, "Gain-scheduled robust fault detection on time-delay stochastic nonlinear systems," IEEE Trans. Ind. Electron., 58(10): 4908–16, 2011.

[17] C. Sloth, T. Esbensen, J. Stoustrup, "Robust and fault-tolerant linear parameter-varying control of wind turbines," Mechatronics, 21(4): 645–59, 2011.

[18] F. D. Bianchi, R. J. Mantz, C. F. Christiansen, "Gain scheduling control of variable-speed wind energy conversion systems using quasi-LPV models," Control Eng. Pract., 13(2): 247–55, 2005.

[19] M. Sami, R. J. Patton, "An FTC approach to wind turbine power maximisation via T-S fuzzy modelling and control," in Proc. 8th IFAC

symposium on fault detection, supervision and safety of technical processes, Mexico City, Mexico, 45(20): 349-354, 2012.

[20] A. A. Ozdemir, P. Seiler, G.J. Balas, "Wind turbine fault detection using counter-based residual thresholding," in Proc. IFAC world congress, 44(1): 8289-8294, 1998.

[21] M. R. Alizadeh Pahlavani, H. Damroodi, "LPV Control for speed of permanent magnet synchronous motor (PMSM) with PWM Inverter," J. Electr. Comput. Eng. Innovations (JECEI), 4(2): 185-193, 2016.

[22] M. Rahnavard, M. R. Hairi-Yazdi, M. Ayati, "On the development of a sliding mode observer-based fault diagnosis scheme for a wind turbine benchmark model," Energy Equip. Syst., 5(1): 13–27, 2017.

[23] J. Liu, D. Xu, X. Yang, "Sensor fault fetection in variable speed wind turbine system using $H-/H\infty$ method," in Proc. 7th World Congress on Intelligent Control and Automation: 4265–4269, 2008.

[24] J. Blesa, P. Jiménez, D. Rotondo, "An interval NLPV parity equations approach for fault detection and isolation of a wind farm," IEEE Trans. Ind. Electron., 62(6): 3794–3805, 2015.

[25] H. Badihi, Y. Zhang, H. Hong, "Fault-tolerant cooperative control in an offshore wind farm using model-free and model-based fault detection and diagnosis approaches," Appl. Energy, 201: 284-307, 2017.

[26] H. Badihi, Y. Zhang, H. Hong, "Active fault tolerant control in a wind farm with decreased power generation due to blade erosion / debris build-up," IFAC, 48(21): 1369–74.

[27] M. Mousavi, M. Rahnavard, M. R. Hairi-Yazdi, M. Ayati, "On the development of terminal sliding mode observers," in Proc. 26th Iranian Conference on Electrical Engineering (ICEE 2018), 2018.

[28] M. Rahnavard, M. Ayati, M. R. Hairi-Yazdi, M. Mousavi, "Finite time estimation of actuator faults, states, and aerodynamic load of a realistic wind turbine," Renew. Energy, 130: 256–267, 2019.

[29] M. Mousavi, M. Rahnavard, M. Ayati, M. R. Hairi Yazdi, "Terminal sliding mode observers for uncertain linear systems with matched disturbance," Asian J. Control, 21(1): 377–386, 2019.

[30] M. Mousavi, M. Rahnavard, S. Haddad, "Observer based fault reconstruction schemes using terminal sliding modes," Int. J. Control, 93(4): 881-888, 2018.

[31] Wonderful Pictures, "Wind turbine pictures from around the world", 2017. [Available online].

[32] A. Pisano, E. Usai, "Globally convergent real-time differentiation via second order sliding modes Globally convergent real-time differentiation via second order sliding modes," Int. J. Syst. Sci., 38(10): 37–41, 2007.

[33] C. P. Tan, C. Edwards, "Sliding mode observers for reconstruction of simultaneous actuator and sensor faults," in Proc. IEEE Conference on Decision and Control, 2 :1455–1460, 2003.

[34] H. Alwi, C. Edwards, "Robust fault reconstruction for linear parameter varying systems using sliding mode observers," Int. J. Robust Nonlinear Control, 24(14): 1947-1968, 2013.

[35] J. A. Moreno, M. Osorio, "Strict lyapunov functions for the super-twisting algorithm," IEEE Trans. Autom. Control., 57(4): 1035–1040, 2012.

[36] S. Sundaram, C. N. Hadjicostis, "Structural controllability and observability of linear systems over finite fields with applications to multi-agent systems," IEEE Trans. Autom. Control, 85(1): 60-73, 2012.

[37] A. Kumar, K. Stol, "Simulating feedback linearization control of wind turbines using high-order models," Wind Energy, 13(5): 419-432, 2010.

[38] G. Pujol-Vazquez, L. Acho, J. Gibergans-Báguena, "Fault detection algorithm for wind turbines' pitch actuator systems," Energies, 13(11): 2861, 2020.

[39] D. DSL, L. PW, "Simulation model of wind turbine 3p torque oscillations due to wind shear and tower shadow," IEEE Trans. Energy Convers., 21(3): 717–724, 2006.

Biographies

Mohammad Mousavi received his B.Sc. degree in mechanical engineering from Shiraz University, Shiraz, Iran, in 2015. In 2017, he graduated from the School of Mechanical Engineering, University of Tehran, Tehran, Iran. He researches in the fields of wind turbines and model-based fault detection in the Advanced Instrumentation Laboratory, at the School of Mechanical Engineering. His current research interests are industrial application of observers, theorical enhancement of sliding mode observers, linear parameter varying observer, and controller design.

- Email: smousav1@binghamton.edu
- ORCID: 0000-0003-2410-4595
- Web of Science Researcher ID: NA
- Scopus Author ID: NA
- Homepage: NA

Moosa Ayati received his B.Sc. degree from Isfahan University of Technology, Isfahan, Iran, in 2004, and his M.Sc. and Ph.D. degrees in 2006 and 2011 from K. N. Toosi University of Technology, Tehran, Iran, all in Electrical Engineering with the first rank honors. He spent two years as a Post-Doctoral Fellow at the University of Tehran School of Electrical Engineering, College of Engineering, Tehran, Iran, working on fault detection systems. He is currently head of the Advanced Instrumentation Laboratory (AIL) and an Associate Professor with the control division, School of Mechanical Engineering, College of Engineering, at the University of Tehran, Tehran, Iran. His area of interest includes adaptive control and system identification, fault detection systems, instrumentation and industrial automation, Mechatronics, and hybrid systems. Professor Ayati is a member of the Iranian Society of Instrumentation and Control, Iranian Society of Mechanical Engineers, and the National Society of Mechatronics.

- Email: m.ayati@ut.ac.ir
- ORCID: 0000-0001-9943-739X
- Web of Science Researcher ID: AFQ-6437-2022
- Scopus Author ID: 25027078800
- Homepage: https://rtis2.ut.ac.ir/cv/m.ayati/?lang=en-gb

Mohammad Reza Hairi-Yazdi received his B.Sc. and M.Sc. degrees in Mechanical Engineering from Amir Kabir University of Technology, Tehran, Iran in 1985 and 1987 respectively. He received his Ph.D. degree from Imperial College London in 1992 and since then he has been at the University of Tehran, Tehran, Iran where he is now a Professor at the School of Mechanical Engineering. His main research interests include design, simulation, manufacturing and control of dynamic systems.

- Email: myazdi@ut.ac.ir
- ORCID: 0000-0002-2507-313X
- Web of Science Researcher ID: NA
- Scopus Author ID: NA
- Homepage: NA

Shahin Siahpour received his B.S. degree in mechanical engineering from Shiraz University, Shiraz, Iran, in 2015, and the M.S. degree in mechanical engineering from University of Tehran, Tehran, Iran, in 2017. He is currently pursuing the Ph.D. degree in mechanical engineering with the University of Cincinnati, Cincinnati, OH, USA. His research interests include deep learning, prognostics, health management, and industrial AI.

- Email: siahposn@mail.uc.edu
- ORCID: 0000-0002-5359-7731
- Web of Science Researcher ID: NA
- Scopus Author ID: NA
- Homepage: NA

How to cite this paper:
M. Mousavi, M. Ayati, M. hairi-yazdi, S. Siahpour, "Robust linear parameter varying fault reconstruction of wind turbine pitch actuator using second order sliding mode observer," J. Electr. Comput. Eng. Innovations, 11(1): 229-241, 2023.

DOI: 10.22061/jecei.2022.8179.500

URL: https://jecei.sru.ac.ir/article_1786.html